WELDING RESEARCH

SUPPLEMENT TO THE *WELDING JOURNAL*, JANUARY 2006
Sponsored by the American Welding Society and the Welding Research Council

A Novel Edge Feature Correlation Algorithm for Real-Time Computer Vision-Based Molten Weld Pool Measurements

An adaptable method of implementing image processing-based upper surface molten weld pool measurements to facilitate closed loop process control is presented

BY C. BALFOUR, J. S. SMITH, AND A. I. AI-SHAMMA'A

ABSTRACT. The design, testing, and implementation of a versatile algorithm developed to provide robust real-time processing of images for use with a vision-based computer control system is discussed. A generic approach to the implementation of the image-processing algorithm has been employed, allowing a wide variety of imaging devices to be used. The particular application of this work involves the implementation of a weld face or upper surface sensor for GTAW process measurement and automation based upon image edge feature detection. The objective is to utilize the measurements generated by the processing algorithm within a feedback-based process control system. This control system is intended to provide active adjustment of the key process control parameters in order to compensate for deviations from a predefined set of reference or "base line" conditions that may occur in practice. This provides an attractive and potentially more efficient alternative to more traditional "open loop" type control schemes that would normally be employed. The combination of this application and the algorithm that has been developed represent a novel use for computer-based image processing.

Introduction

A number of different approaches to weld process automation have been studied over the years (Refs. 1–4). In the past, a series of different techniques such as welding power source waveform characteristic analysis (Refs. 5, 6) have been used to try and correlate changes in voltage and current waveforms with any subsequent deviations in weld quality. Other approaches such as artificial intelligence based methods (Refs. 7, 8) have been used to determine an automated methodology for selecting weld process parameters. A potential drawback with these types of methods is that they may only be applicable for use with a particular welding power source and a specific welding arrangement.

An alternative approach is to use a computer vision-based system to take geometrical measurements during the formation of a weld. A simplified example of an arrangement for a vision sensor for orbital welding is shown in Fig. 1. Positioned in front of the welding torch is a commercial electronic surveillance camera that has a near-infrared filter and optical arrangement that allows a picture of the molten weld pool to be generated. The filter is used to suppress most of arc light by only allowing a limited wavelength range, as dictated by the filter characteristics, to illuminate the molten weld pool and its surrounding area. For most applications, the filter is selected to be in the near-infrared range close to the cut-off wavelength for the camera detector. This reduces the sensitivity of the camera image to fluctuations in the intense arc light generated during the welding process. Analysis of the image generated by the camera system allows measurements of the weld size to be taken during its molten or formation phase.

With any welding configuration, there are often many factors that may contribute to variations in the process conditions and ultimately these may result in weld discontinuities (Ref. 9). Typical problems could include machining tolerances of the components to be welded, cast-to-cast differences in material properties, misalignment of the welding torch, and inaccuracies associated with the workpiece fixturing arrangement. Therefore, a non-contact sensing system to provide measurements that may be used with a feedback process controller in order to counteract some of the problems associated with traditional open loop welding has the potential to significantly improve the reliability of the process.

The general requirement of the work discussed has been to provide an effective and efficient alternative to a more traditional type of approach that would normally rely on a defined set of experimental welds in order to derive a suitable set of weld process parameters. These parameters are usually selected at the beginning of the welding cycle, they have a nonlinear interrelationship, and active compensation of their values would not normally occur during subsequent welding. This leads to a possibility of discontinuities and potential weld failures if deviations in the process conditions occur (Ref. 10).

KEYWORDS

Image Processing
Edge Feature Correlation
Vision Sensor
Weld Face
Real Time
Closed Loop Control
Weld Process Monitoring
Weld Quality Monitoring
GTAW
Weld Process Control

C. BALFOUR (c.balfour@liv.ac.uk*), J. S. SMITH, and A. I. Al-SHAMMA'A are with the Department of Electrical Engineering and Electronics, The University of Liverpool, Liverpool, U.K.*

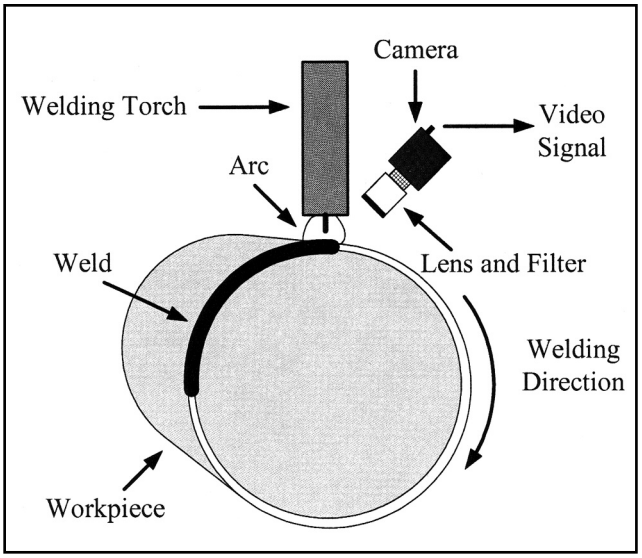

Fig. 1 — A simplified orbital welding arrangement.

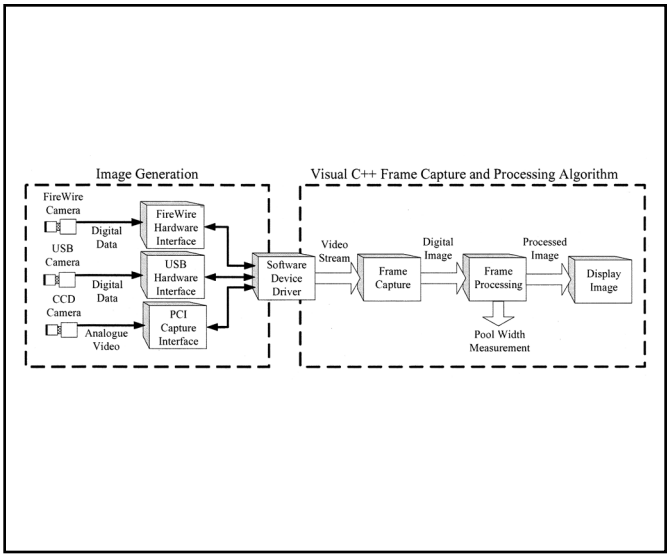

Fig. 2 — PC-based image capture, digitization, and processing.

This paper describes a universal approach for the implementation of a robust algorithm for the analysis of the images from a vision sensor. This has allowed real-time geometrical measurements of the upper surface or "weld face" molten weld pool width to be made for commonly used welding processes such as gas tungsten arc welding (GTAW). An image feature correlation-based image-processing algorithm has been specially developed (Ref. 11). This algorithm may be configured or "trained," by the use of a series of parameters, to cope with some of the fluctuations of image quality that may occur when a vision-based approach is used for this type of application. The processing algorithm has been developed using the Microsoft® Visual C++ (Ref. 12) language using a standard PC environment. The image digitization and processing software has been designed so that it is capable of communicating with a wide variety of modern imaging devices. The emphasis of the work described has been to devise a robust measuring technique that may be used in conjunction with a closed loop process controller.

Image Processing Algorithm Development

The image analysis system was designed using the general specification listed in Table 1. In line with industrial requirements, a Visual C++ based program for the capture and digitization of images from a weld pool observation camera has been developed around a standard PC architecture, as shown in Fig. 2.

Different capture devices may be coupled to the image processing software by using a standard imaging device, its respective interface hardware, and its "device driver" program. The image processing software may then be configured to access the resultant video stream of digitized frames from an imaging device. These digitized frames are then passed to a processing algorithm to perform the image analysis and generate the required measurements at a rate that is within the standard inter-frame display time of 40 ms for a typical commercial camera. Finally, the processed image is displayed on the computer screen.

The image analysis is essentially a further development of a previous image intensity-based weld feature correlation algorithm (Ref. 13). This was originally designed for the spatial domain processing of high-quality welding images that have been captured as a stream of 8-bit grayscale images at a known resolution. The image analysis technique basically uses searching from left to right in a captured image for the closest match to previously stored reference features that represent the pixel intensity profile of the left and right weld pool edges. This is achieved using the general approach specified by Equation 1 (Ref. 13).

$$C_e\left[i\right] = \sum_{j=0}^{Fs} \left| S_f\left[j\right] - I_n\left[i+j\right] \right| \text{for } 0 \le i < I_w \quad (1)$$

where C_e is an array holding the correlation error values, S_f is an array of F_s elements to store the intensity levels of a feature extracted from a reference image. I_n

Table 1 — Image Processing System Specification

Attribute	Description
Computer	Standard PC
Processor	2.5 GHz Pentium 4
Memory	512 MB
Graphical Display	AGP interface
Camera	Pulnix TM6EX, Webcam, or PixeLINK
Image capture device	PCI card, USB, or FireWire
Nominal capture resolution	640 × 480 pixels, 8 bit greyscale
Framing processing rate	25 Hz
Operating system	Windows 2000

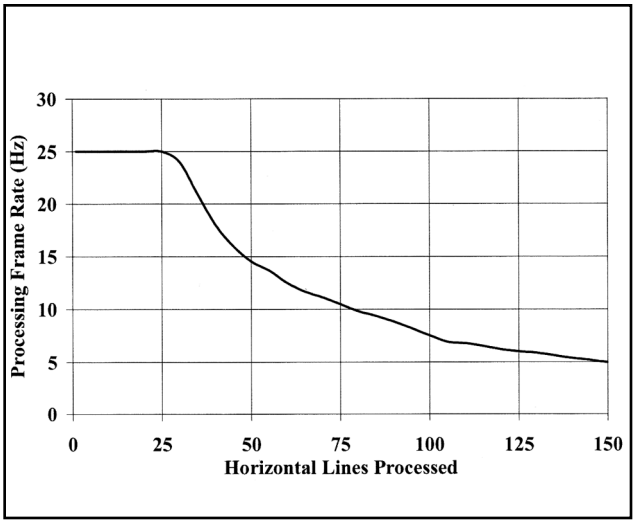

Fig. 3 — Frame processing rate vs. lines processed.

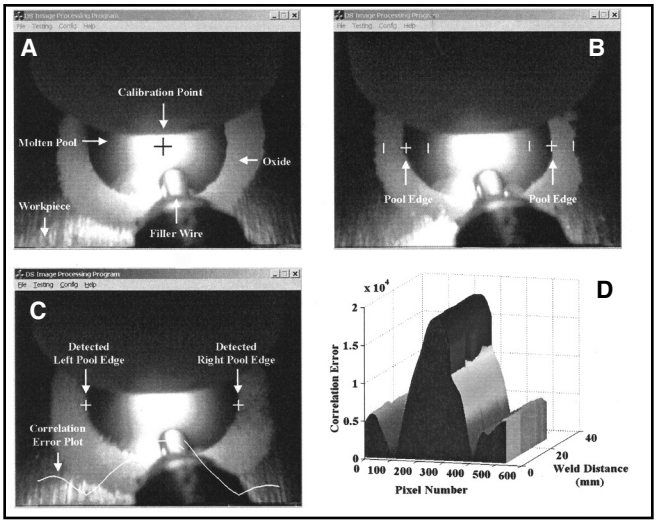

Fig. 4 — Feature correlation for AC GTA weld pool width measurement. A — Image calibration; B — feature extraction; C — feature correlation; D — correlation surface.

is an array of intensity levels from the digitized image taken from left to right at the vertical calibration position, I_w is the width of the image in pixels, and F_m is the value of least correlation error.

When the calculations specified by Equation 1 have been completed, the horizontal position of best correlation along the image to which the stored feature may be matched, F_m, may be found, as specified by Equation 2 (Ref. 13). The position at which this minimum value occurs along the correlation error array C_e represents the position along the image from left to right at which the best match occurs.

$$Fm \leftarrow min \left\{ C_e[i] \text{for } 0 \le i < I_w \right\} \quad (2)$$

A potential drawback of using this approach is that to search an entire image may involve a significant amount of processing. To illustrate this, a graph of the image processing algorithm frame processing rate as a function of the number of horizontal lines processed for a image resolution of 640 × 480 pixels using a PCI capture card is shown in Fig. 3.

The graph shown in Fig. 3 clearly demonstrates that the volume of data to be processed needs to be restricted to 25 horizontal lines or less in order to generate a measurement at the frame rate of the imaging device. Several techniques have been used to achieve this in order to allow real-time processing. To reduce the amount of processing required, the left edge feature is only searched for to the left of the calibration position. Similarly, right feature searching takes place to the right of the calibration position. Accurate alignment of the imaging camera removes the need to scale, rotate, or move the position of reference features relative to a live image to be processed, limiting the amount of processing required. Positional calibration has also been used to identify a particular area of an image that is to be processed.

The basic operation of the algorithm is illustrated in Fig. 4 for a sequence of images using the AC GTAW process on aluminum. A calibration point, as shown in Fig. 4A, is set in the center of a reference image to indicate the specific area about which the processing of subsequent images should take place. Following the calibration of the algorithm, a pair of edge features are extracted from a sample image as shown in Fig. 4B. The crosses represent the center of the feature to be extracted, and the vertical bars to the left and right of each feature represent the size of the feature. Once this information has been provided, the algorithm is configured for real-time operation so that 'live' image processing and measurements may then be made. Figure 4C shows a processed image where the cursors indicate the measured position of the weld pool edges and the trace below the calibration point shows a normalized plot of the correlation error. The two troughs immediately below each weld pool edge represent the positions of least correlation error, and hence, the most likely positions of the weld pool edges. A surface plot of absolute value of the correlation error for a weld sequence is shown in Fig. 4D, where the points of least correlation error are clearly shown at 100 and 400 pixels along the image. The difference between the two measured edge points represents the weld pool width. Regulation of the molten weld pool width by a process controller may be used to provide an effective

Table 2 — Tested Image Capture Device Frame Processing Benchmarks

Camera	Detector	Interface	Maximum Resolution	Frame Processing Rate (Hz)
PixeLINK PL-6A41	CMOS	Firewire	1280 × 1024	12
Pulnix TM6EX	CCD	Hauppauge Win TV PCI	640 × 480	25
Mri WebCam	CMOS	USB	640 × 480	12
Pulnix TM526	CCD	Hauppauge Win TV USB	240 × 358	25

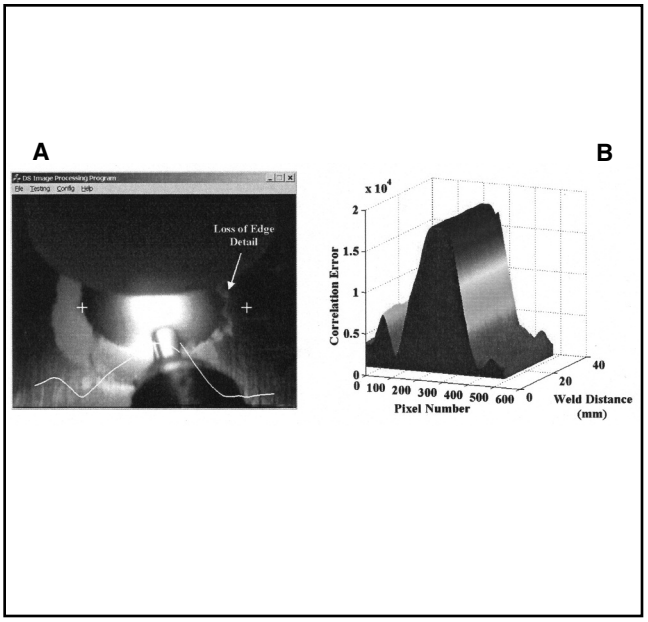

Fig. 5 — Reduction in image quality. A — Processed image B — correlation surface.

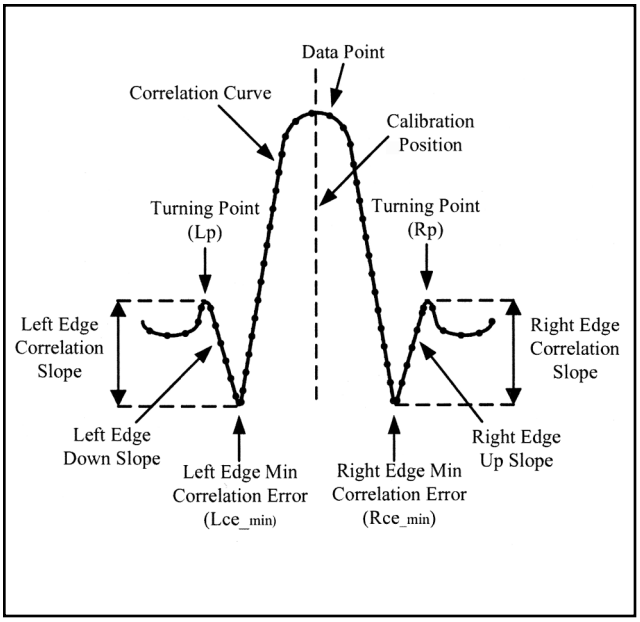

Fig. 6 — Correlation trough analysis.

Table 3 — Welding Parameters

Parameter	Value
Process	AC GTAW at 100 Hz
Material	1.6 mm thick 2024, T4 aluminum
Welding electrode	3.2 mm Zr tungsten
Shielding gas	Pure argon at 10 1/min
Welding speed	3.3 mm/s
Nominal welding current	80 A
Welding wire	1.2 mm type 5356 at 15 mm/s
Imaging filter	950 nm ± 13.3 nm

means of stabilizing the welding conditions and hence producing more consistent and repeatable welds.

In practice, there are many factors such as changes in the workpiece surface finish, light reflection, movement of the molten weld pool, and variations in the arc light intensity that may contribute to degradation in the quality of the image to be analyzed. Therefore, a potential drawback with this approach is that a reduction in image quality may produce incorrect measurements, as illustrated in Fig. 5. The image in Fig. 5A shows loss of oxide on the right-hand side of the weld pool, leading to loss of edge detail and incorrect measurement of the position of the edge feature. This problem is shown by the "flattening" or distortion of the correlation surface on the right-hand side of Fig. 5B.

To address the problem of image quality variation, an enhanced processing algorithm that effectively analyzes, per frame, the degree of correlation to a particular feature has been devised. A poor quality image can then be detected, allowing a series of rules to be subsequently applied so as to avoid inaccurate measurements from being generated. Figure 6 illustrates a simplified two-dimensional form of a typical correlation curve of matching errors for left and right edge features in a processed frame. For the left edge feature, the number of correlation error points that exist from the minimum correlation error location to the next turning point or nonincrease in error value when moving to the left is calculated. The value of correlation error at the turning point is also recorded. In a similar manner, the number of points in the slope of the right feature correlation curve moving to the right of the minimum correlation error location is recorded. Following this, the percentage change in correlation value from the minimum correlation error to the turning point for each feature is then calculated. This percentage change in correlation error relative to the minimum value and the number of slope points before a turning point is reached are used as parameters to determine the strength of correlation for a particular edge feature. Careful selection of the ranges of these values allows discrimination between acceptable and poor feature matches to be made by effectively detecting when correlation edge flattening or distortion takes place. This provides a simple and efficient mechanism to detect when image quality degradation occurs.

Equations 3 and 4 define expressions for the percentage change in the correlation slopes for the left and right edges.

$$Lcc = \frac{Lp - Lce\_min}{Lce\ \ min} \times 100 \quad (3)$$

where Lcc is the left correlation change in percent, Lp is the peak correlation error at the left correlation down slope turning point, and Lce_min is the minimum left correlation error.

$$Rcc = \frac{Rp - Rce\_min}{Rce\_min} \times 100 \quad (4)$$

where Rcc is the right correlation change in percent, Rp is the peak correlation error at the right correlation up slope

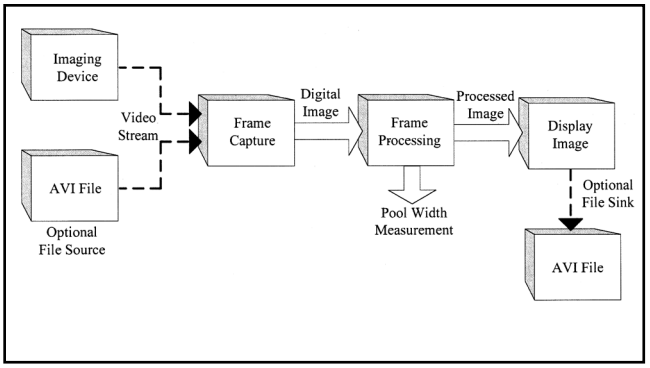

Fig. 7 — Image processing capture graph.

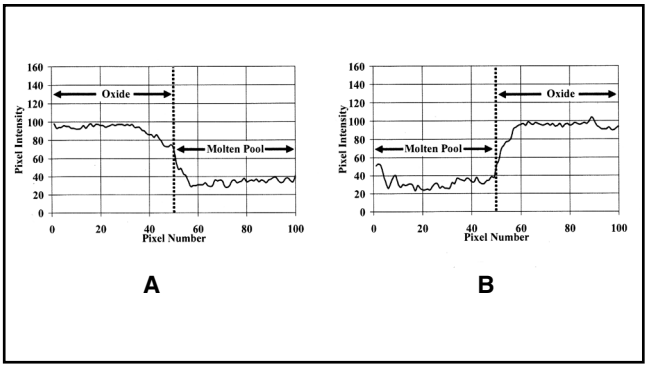

Fig. 8 — Reference edge features. A — Left edge; B — right edge.

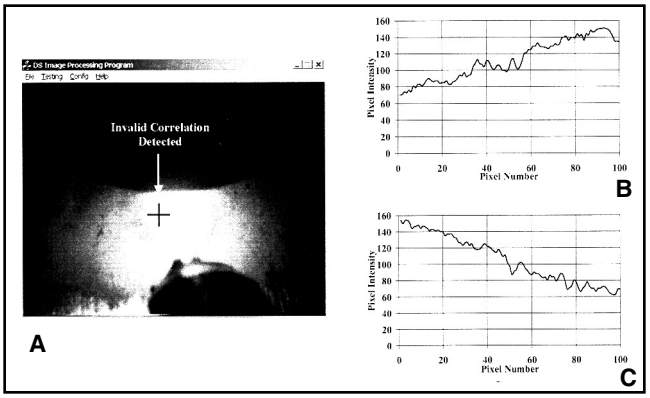

Fig. 9 — Initial weld pool. A — Sample image; B — left edge intensity profile; C — right edge intensity profile.

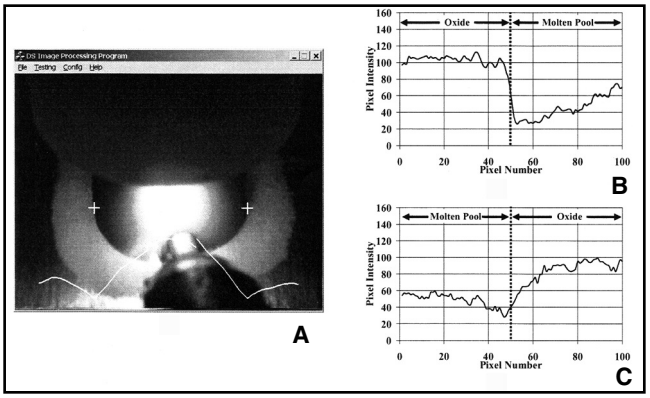

Fig. 10 — Good quality weld pool image. A — Captured image; B — left edge intensity profile; C — right edge intensity profile.

turning point, and Rce_min is the minimum right correlation error.

A valid correlation for a left edge image feature occurs when Lcc and the number of error points or samples in the left correlation down slope are above predefined values or thresholds. In a similar manner, a valid correlation for a right edge image feature occurs when Rcc and the number of right edge up slope points are above predefined threshold values.

The final phase of processing is to decide what action to take when image quality degradation is detected. If an invalid edge or edges are detected when the algorithm is initialized, the difference between the center points of the two features used to configure the algorithm, as previously shown by the crosses in Fig. 4B, is returned as the initial or default pool width value. If an invalid edge is detected, following at least one successful pool width measurement, then the last known acceptable pool width is used as the algorithm output. This will continue for each frame processed by the software until an updated measurement can be made.

Software Implementation

The software for the image-processing program has been developed using Microsoft® Visual C++ on a standard PC. To access digitized video from a capture device, the Microsoft® ActiveX® DirectShow (Ref. 14) programming interface has been used. This allows interaction with a stream or sequence of digitized video from a standard capture device that conforms to the Windows® Driver Model or WDM device driver interface (Ref. 15). The general approach is to develop software that defines how interaction with a digitized video stream will take place using a capture graph. A simplified form of the image processing capture graph that has been developed is shown in Fig. 7.

An imaging device or a previously recorded audio video interleave (AVI) file (Ref. 16) may be configured to act as a digital video source. The processing software may then be used to analyze the resultant video stream by processing each frame to produce the required measurements. The processed frames are then supplied as a video stream for display and, if required, the processed video may also be saved to file in AVI format. Table 2 lists the devices that have so far been used to capture video. Benchmarking tests were used to find the processed frame rate that could be achieved at the maximum capture resolution, as specified in Table 2. This provides an indication of the performance limits of the capture and processing system for a particular imaging arrangement. For the PixeLINK camera, a frame rate of 25 Hz may be achieved by using a capture resolution of 640 × 480 pixels or lower. Similarly, the WebCam capture frame rate may be increased to 25 Hz by reducing the capture resolution to 320 × 240 pixels.

The general procedure used to configure the image processing software would be to save a video sequence of captured images to an AVI file from a set of calibration or reference welds. These files may then be played through the capture and processing software so that the software may be configured, as described in the previous section, to produce a reliable measurement of the weld pool width. Alternatively, if the imaging device used has a video output signal such as composite video, then the reference images may be archived to media such as videotape. The recorded images may then be played back through the processing software by using a capture device that has an appropriate interface, such as a television interface or WinTV card, to convert the recorded images into a digital video stream. Once this configuration and calibration process is complete, the image processing software

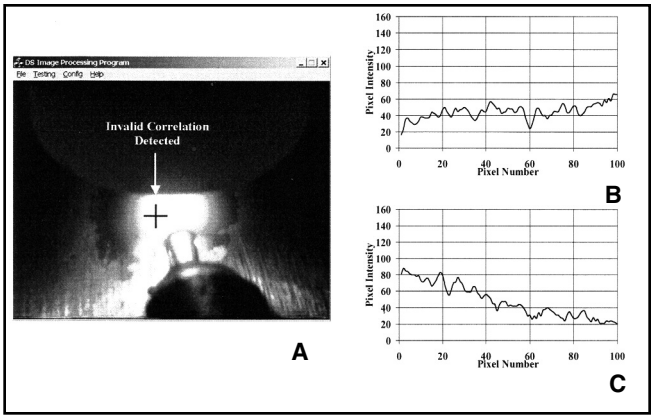

Fig. 11 — Loss of edge detail. A — Captured image; B — left edge intensity profile; C — right edge intensity profile.

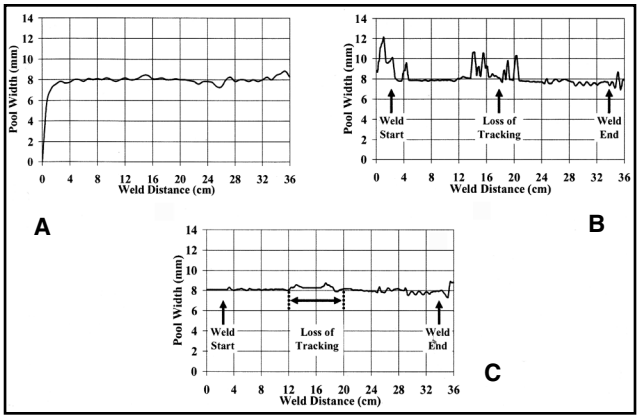

Fig. 12 — Comparison of pool width measurements. A — Manually measured; B — no correlation slope testing; C — correlation slope testing.

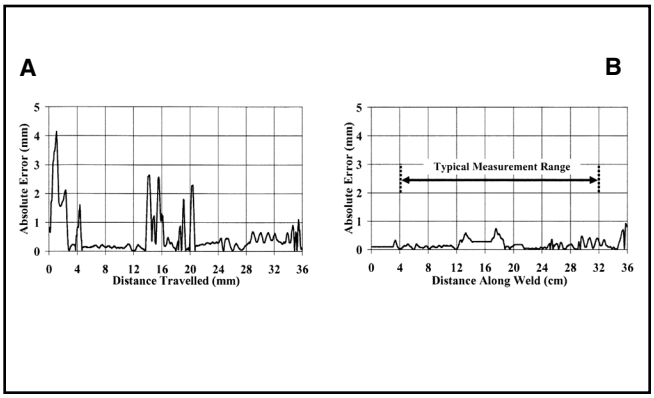

Fig. 13 — Comparison of automated weld pool width measurement absolute error. A — Without correlation shape testing; B — with correlation shape testing.

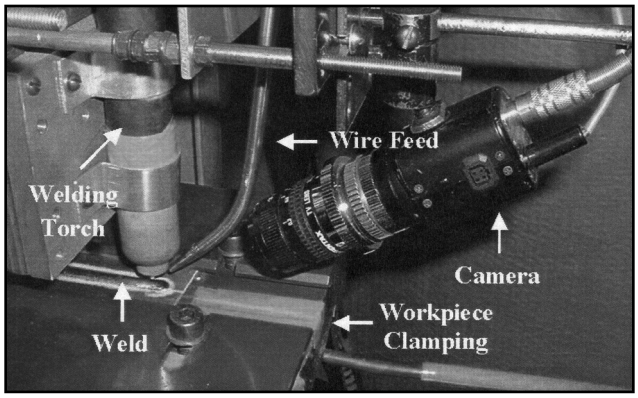

Fig. 14 — Experimental welding system.

Table 4 — Correlation Algorithm Settings

Parameter	Value
Left edge feature size (pixels)	100
Min left correlation error change (%)	40
Min left correlation slope points	30
Right feature size (pixels)	100
Min right correlation error change (%)	40
Min right correlation slope points	30

may then be used to process live images and provide measurements in real time.

Experimental Procedure and Results

To evaluate the performance of the enhanced correlation algorithm, a recording of a previously controlled weld was made that used the process parameters listed in Table 3. This weld had a nominal upper pool width of 8 mm and the images generated exhibited periodic degradation in image quality and subsequent loss of feature detail, making the image sequence suitable for testing the operation of the image processing software.

A sequence of captured images and edge feature graphs were then used to demonstrate the operation of the correlation slope-testing algorithm when it was configured with the empirically derived parameters listed in Table 4. Following this, an evaluation of the accuracy of the automated pool width measurements was made with and without correlation slope testing. This was achieved by comparing the algorithm measurement results with manually made postweld readings of the true weld pool width.

Graphs of the left and right reference edge feature intensity profiles for a high-quality image of AC GTAW on aluminum plate are shown in Fig. 8. For the reference features, a clear transition at the edge of the molten weld pool can be seen. The left edge exhibits a transition from a lower to higher intensity at the molten weld pool edge, with the converse of this occurring for the right edge.

An extreme test for the correlation slope detection algorithm is shown in Fig. 9, where the weld pool is beginning to be established at the start of the weld cycle. The algorithm has detected a problem with the shape of the sampled edge features and indicated this by placing a large

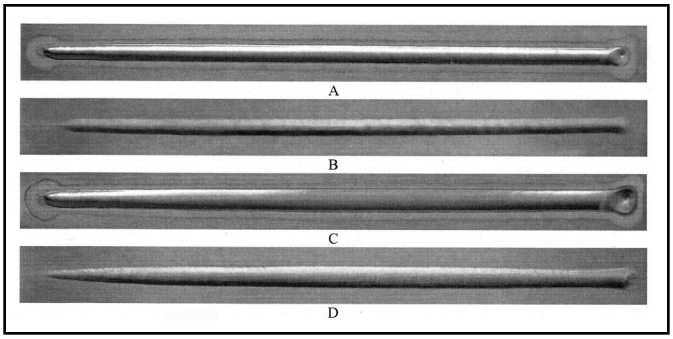

Fig. 15 — AC GTAW on aluminum. A — Controlled upper surface; B — controlled lower surface; C — uncontrolled upper surface; D — uncontrolled lower surface.

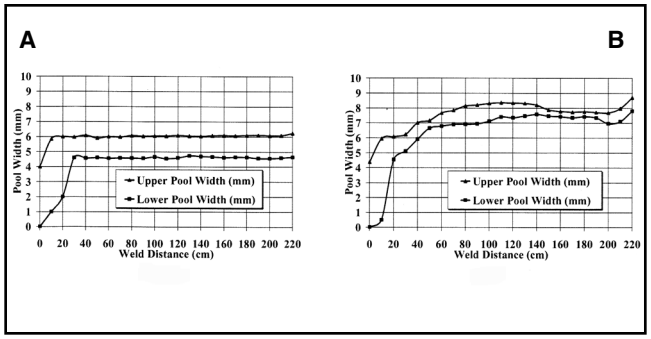

Fig. 16 — Pool width graphs. A — Controlled pool widths; B — uncontrolled pool widths.

cursor on the left side of the image. The flattening of the edge features and an increase in the overall intensity indicates a poor quality of image, as shown in Fig. 9B. This results in a ramp-like profile, with no clear discontinuity in intensity level at the weld pool edges. For this condition, a default pool width consisting of the horizontal difference between the two reference feature extraction center points is used as the weld pool width measurement.

When the molten weld pool has been established, a measurement may be reliably made as soon as clear edge features exist, as shown in Fig. 10. The general form of the graphs in Fig. 10B and C show a close resemblance to the reference features in Fig. 8, so a reliable measurement can be made.

If reduction in the image quality and subsequent loss of the edge feature detail occurs, as shown in Fig. 11, then this may be detected by the flattening of the edge intensity profiles. For this case, the algorithm outputs the last successful measurement until a new measurement can be made or the weld sequence completes. The large cross to the left of the center of the image provides a visual indication that the correlation test has failed.

If the field of view of the imaging device and its capture resolution are known, then this measurement may be translated into millimeters as specified in Equation 5. This allows comparisons between the automated image processing measurements and postweld manual measurements to be made.

$$Pw\_mm = \frac{Pw\_pix}{Sw\_pix} \times Iw\_mm \qquad (5)$$

where Pw_mm is the pool width in mm, Pw_pix is the measured pool width in pixels, Sw_pix is the screen width in pixels, which is governed by the capture resolution used, and Iw_mm is the measured width of the camera field of view in mm.

The plots shown in Fig. 12 provide a comparison between the weld pool width measurement stability with and without correlation slope testing in relation to a set of manually measured points of the actual weld pool width that show a typical nominal pool width of 8 mm. The graphs clearly show the improvement in the stability and accuracy of the measuring technique when correlation slope testing is used. The labels on the graphs shown in Fig. 12B and C indicate key phases of the measurement sequence. As shown, the molten weld pool has been fully established after about 3 cm along the weld. Prior to pool establishment, the noncorrelation testing pool width graph shown in Fig. 12B indicates that an unstable measurement is produced. When loss of edge tracking occurs between approximately 12 and 20 cm along the weld, due to intermittent degradation in the image edge feature detail, an unstable measurement is produced when correlation slope testing is not used. After a distance of about 34 cm along the weld the end of the welding sequence is approaching and the size of the molten weld pool begins to decay, resulting in poor edge tracking. The graph of the measurement produced when correlation slope testing is used, as shown in Fig. 12C, has produced a significantly more stable measurement. At the start of the weld sequence the default pool width of the difference between the locations of the reference edge features is used. When a subsequent image is processed that exhibits loss of edge detail then the last successfully measured weld pool width is used until the measurement can be reestablished.

A plot of the relative measuring accuracy for the correlation slope testing and noncorrelation slope testing measurement methods in relation to the manually measured nominal weld pool size of approximately 8 mm is shown in Fig. 13. A variation in excess of 4 mm in the measurement is produced without correlation slope testing, as shown in Fig. 13A. The graph of the absolute measuring error in Fig. 13B clearly shows a significant improvement in the accuracy and stability of the measurement generated when correlation shape testing is used resulting in a measurement to within 1 mm of the actual value. This improvement has been achieved for a digitized sequence of weld images that exhibit a tendency for significant variations in image quality and thus represents an extreme test for the processing algorithm.

The typical measuring range for process control applications has also been indicated in Fig. 13B. For process control, a start delay would normally be used to allow the weld pool to establish. Following this, feedback process control may then be activated using a timing or synchronization signal from a weld sequencer. The process controller will then regulate the upper weld pool width based upon the measurements from the image-processing algorithm. This is achieved by making appropriate adjustments to the process parameters in response to any detected deviations in the measured pool width from a "setpoint" or target value. At the end of the welding path, a synchronization signal is then used to turn off the controller just before the weld terminates.

A labeled photograph of the experimental welding apparatus used to undertake trial welds using an upper surface vision sensor and image processing based real-time weld pool width measurements is shown in Fig. 14. The welding system consisted of a horizontal workpiece clamping arrangement and a vertically mounted welding torch with a welding wire delivery assembly positioned in front of the torch. A Pulnix® CCD camera (35 mm in diameter and 50 mm in length), a 16-mm C-mount focal length lens, and a 950-nm near-infrared bandpass filter with a half wavelength of 13.3 nm and a peak transmission of 45% were mounted in front of the welding torch. This arrangement was used to generate an image of the

upper surface molten weld pool that was suitable for processing.

Photographs of the upper and lower surfaces of a controlled and an uncontrolled weld are shown in Fig. 15. Both of the welds used the baseline parameters specified in Table 3. For the controlled weld shown in Fig. 15A and B, the upper surface measured weld pool width regulated to a target size of 6 mm. This was achieved using proportional and integral or PI-based control (Ref. 17), with experimentally determined values for the proportional and integral gain. The PI controller, as specified in Equation 6, was used to control the welding current based upon measurements of the weld pool width supplied by the correlation-based image-processing algorithm. This feedback control action effectively adjusted the heat input to the process in response to any detected deviations in the upper weld pool width, which subsequently produced a more uniform and consistent weld. The control action also has an impact on the regularity of the lower side weld bead, as shown in Fig. 15B. This contrasts with the uncontrolled weld that is shown in Fig. 15C, D. The uncontrolled weld exhibits variations in upper and lower surface weld pool width due to such factors as heat buildup during welding and nonuniformity of the heat sinking provided by the workpiece fixture arrangement.

$$I_{adj} = K_p e_{pw} + K_i \int e_{pw} \qquad (6)$$

where I_{adj} represents the welding current adjustment, K_p is the proportional gain, e_{pw} is the pool width error defined as the difference between the target and measured upper surface pool width, and K_i is the integral gain based upon the last x samples, where x is an integer in the range 1 to 100.

This difference between the regularity of the controlled and uncontrolled welds can be clearly observed by comparing the profile of graphs for the manually measured controlled and uncontrolled post-weld bead widths shown in Fig. 16. For the controlled weld shown in Fig. 16A, a uniform upper and lower bead profile is produced along the weld length. For the uncontrolled weld measurements shown in Fig. 16B, a significant variation in the upper and lower weld pool widths was observed.

Discussion and Conclusions

This paper describes the implementation of a robust image correlation algorithm suitable for welding applications. The principal requirement was to address some of the practical problems of variations in image quality that may be encountered when upper surface weld pool imaging is used. The subsequent testing and analysis of the processing algorithm has shown how reliable geometrical weld pool measurements may be made and images that exhibit degradation in image quality and subsequent loss of feature detail may be tolerated. The use of analysis of the correlation error profile has provided a parametric mechanism to distinguish when image quality degradation has occurred. The technique employed has been designed to have a low computational processing overhead so that the critical requirement of real-time measurement can be maintained. While this technique will not introduce or improve detail in a poor-quality image that exhibits loss of feature information, it does provide an organized method of detecting and coping with this problem. This ultimately results in a more stable and reliable measuring technique as clearly illustrated in the results section. An extensive set of programmable configuration parameters has resulted in a generic and robust processing technique that may be trained to cope with a wide range of images. Therefore, the algorithm that has been developed is considered to represent a significant advancement over previously published methods. It is envisaged that applications for this correlation-based image feature identification approach may exist outside of real-time weld image processing.

A modern visual programming environment combined with ActiveX® technology has resulted in reconfigurable image processing software that is capable of using a broad range of modern commercial capture devices. This has allowed the implementation of a cost-effective frame capture and analysis system by avoiding the use of potentially expensive dedicated or designed-for-purpose systems.

Future research will investigate the feasibility of implementing the enhanced correlation-based approach to weld face sensor image analysis as an embedded processor system. This should allow a compact sensor system to be produced that may be interfaced to a wide variety of modern commercial weld process controllers and imaging devices.

Acknowledgment

The authors wish to thank the EPSRC for the provision of funding in order to carry out this feasibility study.

References

1. Kim, J. W., and Na, S. J. 1993. A self-organizing fuzzy control approach to arc sensor for weld joint tracking in gas metal arc welding of butt joints. *Welding Journal* 72 (2): 60-s to 66-s.

2. Jeng, J. Y., Mau, T. F., and Leu, S. M. 2000. Prediction of laser butt joint welding parameters using back propagation and learning vector quantization networks. *Jnl. Mater. Process Tech.* 99 (1–3): 207–218.

3. Luo, H. Devanathan, R., Wang, J., Chen, X., and Sun, Z., 2002. Vision based neurofuzzy logic control of weld pool geometry. *Sci. Tec. Weld Join.* 7(5): 321–325.

4. Gao, J., and Wu, C. 2001. Experimental determination of weld pool geometry in gas tungsten arc welding. *Sci. Tech. Weld Join.* 6(5): 288–292.

5. Adolfsson, S., Bahrami, A., Bolomsjo, G., and Cleason, I. 1999. On-line quality monitoring in short-circuit gas metal arc welding. *Welding Journal* 78(2): 59-s to 73-s.

6. Quinn, T. P., Smith, C., McCowan, C. N., Blachowiak, E., and Madigan, R. B. 1999. Arc sensing for defects in constant-voltage gas metal arc welding. *Welding Journal* 78(9): 322-s to 328-s.

7. Casalino, G., Hu, S. J., and Hou, W. 2003. Deformation prediction and quality evaluation of the gas metal arc welding butt weld. *Proc. of Inst. of Mech. Eng. Part B, Jnl. of Eng. Manuf.* 217(11): 1615–1622.

8. Kim, I. S., Son, J. S., and Yarlagadda, P. K. D.V. 2003. A study on the quality improvement of robotic GMA welding process. *Robotics and Compu. Int. Manf.* 19(6): 567–572.

9. Gourd, L. M. 1980. *Principles of Welding Technology*. London, Edward Arnold.

10. Lancaster, J. F. 1999. *Metallurgy of Welding*. Cambridge, England: Abington Publishing, Chapter 6.

11. Teuber, J. 1993. *Digital Image Processing.* Hemel Hempstead, England, Prentice-Hall, Chapter 5.

12. Bates, J. G., and Tompkins, T. 1999. *Practical Visual C++ 6*. Indianapolis, Que.

13. Balfour, C., Smith, J. S., and Amin-Nejad, S. 2004. Feature correlation for weld image-processing applications. *Int. Jnl. of Prod. Research* 42(5): 975–995.

14. Pesce, M. D. 2003. *Programming Microsoft® DirectShow® for Digital Video and Television*. Microsoft Press.

15. Oney, W. 2002. *Programming the Microsoft® Windows® Driver Model*. Microsoft Press.

16. Johnson, N., Weiskamp, J., Gault, F., and Florence, M. 1994. *How To Digitize Video*. New York, N.Y.: Wiley, Chapter 15.

17. Raven, F. H. 1987. *Automatic Control Engineering*. New York, N. Y.: Mcgraw-Hill, Chapter 4.